Critical Absorption at Terahertz Frequencies through Fabry–Perot Cavity Resonators

Edoardo Negri, *Member, IEEE*, Dimitrios C. Zografopoulos, Francesco Maita, Luca Maiolo, Romeo Beccherelli *Member, IEEE*, and Walter Fuscaldo *Senior Member, IEEE*

***Abstract*—Critical absorption in planar resonators is achieved when material losses match radiative losses. In this work, we show that this condition can effectively be satisfied by exploiting the higher-order leaky-mode resonances of a metasurface-based Fabry–Perot cavity. Remarkably, *leaky-wave theory* reveals how the condition of maximum power radiated at broadside (typically employed for leaky-wave antennas) is linked to that of maximum absorption (typically employed for absorbers): the two conditions almost coincide in low-loss systems, but progressively differ as the losses increase. To corroborate our design, the reflection spectrum of a Fabry–Perot cavity resonator—consisting of a grounded dielectric slab covered with a subwavelength two-dimensional lattice of metallic strip gratings—is measured through terahertz (THz) time-domain spectroscopy in reflection mode. Importantly, the matching condition for critical absorption is satisfied through the dielectric spacer losses and not the almost lossless metallic metasurfaces. The experiment recorded an impressive -40 dB reflectance spectrum and a nearly step-like π jump of the phase reflection spectrum at around 357 GHz, in agreement with the theoretical expectations for the first-order mode resonance. The proposed metasurface-based Fabry–Perot resonator offers significantly higher flexibility and reliability with respect to conventional absorbers based on thin conducting films, whose design is often hindered by material and fabrication uncertainties.**

***Index Terms*—Critical Absorption, Leaky Waves, Metasurfaces, THz Devices, THz Absorber**

I. Introduction

THE significant advancement of the terahertz (THz) technology [1], especially in the high-demanding sectors of imaging [2] and wireless communications [3], is recently posing the problem of unwanted electromagnetic pollution at THz frequencies in specific environments. Therefore, high-absorption, THz-radiation shielding is one of the milestones that has to be reached for the further development of THz technology [4]. For this reason, different kinds of THz *absorbers* have been recently proposed, some also offering with reconfigurable and broadband features (see, e.g., [5] and references therein).

In this paper we focus on innovative single-band absorbers, which can be extremely useful in specific, sharp-filtering applications, such as thermally based THz imaging [5]. This kind of absorbers is commonly based on some *resonance* mechanisms. For instance, the working principle of the first THz absorber [6]—constituted by a bilayer unit-cell structure—mainly relies on the electric response of split-ring resonators on top of a dielectric slab with some metal strips on the bottom (replaced in follow-up studies by an entire metal plate [7]) which prevent the incident wave to pass through the device [5]. The absorptance in [6] was, however, relatively low, namely 70%.

A 100% absorptance can be theoretically achieved by exploiting a Salisbury screen or the *critical-coupling* phenomenon. The former is an absorber made of a resistive sheet placed a quarter wavelength above a metal ground plane, achieving maximum absorption when the reflected waves cancel out (in phase): its performance, however, strongly depends on the thickness and the features of the available materials [8]. The latter is an effect that can be verified in one-port resonators, i.e., devices backed with a perfect reflector [9]. Such a critical-coupling phenomenon has been studied at optical and THz frequencies through different mechanisms in thin devices [10], such as bound states in continuum [11] and guided resonances [12], metal-insulator-metal [13] or metal-semiconductor-metal [14] cavity resonances, absorbing films [15]–[17], graphene patterning [18], or polarization matching [19]. From a practical viewpoint, the critical-coupling condition occurs when all the power incident on the device is resonantly absorbed (in the structure) [9]. This means that the radiation rate of the resonator has to be equal to the dissipation rate in the device [8], [13], [20]. A common architecture able to reach this condition is constituted by a *thin* grounded dielectric slab with a frequency selective surface (FSS) on top, which interacts with the cavity fundamental mode [13], [21].

This paper demonstrates how the critical-absorption condition can be efficiently reached through the higher-order resonances of a Fabry–Perot cavity (FPC). The latter is constituted by a grounded dielectric slab with a partially reflecting sheet (PRS) on top, which consists of a *homogenized metasurface*, viz., a periodic arrangement of metallic elements

Manuscript submitted October 29, 2025. This work has been partially supported by the project Microtech_for_Green, - CUP 3C22002390006, funded by the Italian Ministry of the Enterprises and of the Made in Italy (MIMIT) - Fondo IPCEI. The work of Dimitrios C. Zografopoulos was supported by the European Union, Next GenerationEU, through the Project "Ecosistemi dell'Innovazione"—Rome Technopole of the Italian Ministry of University and Research, public call n. 3277, PNRR—Mission 4, Component 2, Investment 1.5, under Grant ECS00000024. (*Corresponding author: Edoardo Negri*.) The authors are with the Consiglio Nazionale delle Ricerche, Istituto per la Microelettronica e Microsistemi, 00133 Rome, Italy (e-mail: edoardonegri@cnr.it, dimitrios.zografopoulos@cnr.it, francesco.maita@cnr.it; luca.maiolo@cnr.it, romeo.beccherelli@cnr.it, walter.fuscaldo@cnr.it). D. C. Zografopoulos is also with the Aristotle University of Thessaloniki, School of Electrical and Computer Engineering, 54124 Thessaloniki, Greece.

Manuscript received October 29, 2025; revised December 27, 2025.

with periodicity p much smaller than the operative vacuum wavelength λ_0. As opposed to previous absorbers available in the literature, the metasurface on top of the grounded dielectric slab does not present an inherent resonance, but presents a uniform, collective response represented by a scalar, purely imaginary, sheet impedance $Z_s = jX_s$ [22]. The resonance condition in the proposed FPC-resonators (FPCR) absorbers is thus not related to a specific metasurface geometry but rather to the collective response of the FPC-based device, which provides high resilience to PRS-fabrication tolerances (slight variations, either in the dimensions or the periodicity, among the unit cells have negligible impact on the entire metasurface electromagnetic behavior) and great flexibility in material selection. Being essentially lossless, the metasurface can be fabricated using any noble metal or highly conducting material, without strict requirements on the exact conductivity value. Instead, absorption occurs in the dielectric spacer, which can be selected among readily available materials, as we will show. As a consequence, the proposed technique for designing FPCR critical absorbers provides different degrees of freedom in terms of dielectric slabs and PRS implementation, in stark contrast with absorbers based on thin conducting films (TCFs), typically constrained by the uncertainties that characterize the latter (see, e.g., [8] and references therein).

Remarkably, we exploit leaky-wave theory (Section II) to link the condition for the maximum power radiated at broadside (typically employed for FPCR leaky-wave antennas) to that of maximum absorption (typically employed for absorbers). These two conditions are shown to be equivalent under the assumption of low losses, and slightly differ for moderate to high losses. Thanks to this rigorous theoretical framework, analytical formulas and efficient numerical procedures are provided to finely engineer the metasurface properties to achieve normal-incidence critical coupling through leaky modes of any order supported by the FPCR. It is worth noting that, while increasing the incident angle θ_i on the same FPCR absorber generally leads to a degradation of the absorption performance, the proposed theoretical design framework can be extended to arbitrary values of θ_i.

Although the proposed method is completely general and can be adapted in any frequency range (from microwaves and millimeter waves to optics), a prototype is finally realized and experimentally validated at THz frequencies to test the proposed innovative absorbing device (Section III). In particular, a grounded dielectric slab of a commercial FR-4 is covered with a metal strip grating metasurface, precisely designed to match the higher-order leaky mode of the FPCR. Measurements based on THz time-domain spectroscopy (TDS) working in reflection mode demonstrate the critical absorption of the device through a reflection coefficient as low as -40 dB and a step-like phase profile at the working frequency of 357 GHz. A short discussion (Section IV) concludes the paper.

II. Theoretical Analysis and Numerical Results

A. Theoretical Framework

We consider an FPCR consisting of a grounded dielectric slab covered with a periodic arrangement of subwavelength metallic scatterers, operating in the THz range [23]. Specifically, the periodicity p of the unit cell is set to $p = \lambda_0/5$, with $\lambda_0 = 1$ mm being the operating wavelength at $f_0 = 300\,\mathrm{GHz}$. In this scenario, the PRS is completely represented by a surface impedance boundary condition (SIBC), viz., by an equivalent sheet impedance Z_s [22]. If losses and polarization cross-coupling effects are negligible, as is customary for simple, symmetric PRS unit cells at THz frequencies [23], [24], the SIBC is represented by a scalar and purely imaginary sheet impedance $Z_s = jX_s$ or, equivalently, by a sheet admittance $Y_s = jB_s$, with $B_s = -1/X_s$. Specifically, as the PRS is more reflective, $|X_s|$ tends to zero while $|B_s|$ tends to infinity. The reactance/susceptance $\pm$ sign, instead, depends on the inductive or capacitive character of the unit cell [25]. The attention in this work is focused on inductive-like PRS, such as metal strip gratings [26] and fishnet-like metasurfaces [23], but the proposed design procedure is also applicable in the case of capacitive PRS.

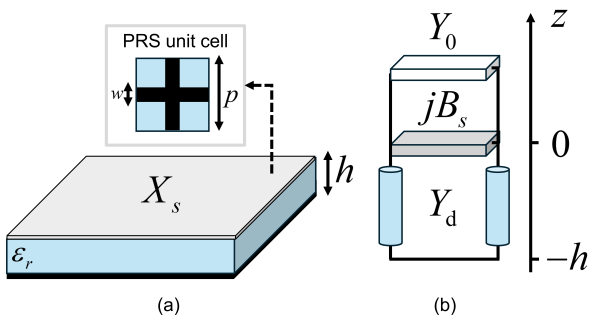

Fig. 1. (a) Schematic representation of the Fabry–Perot cavity resonator working as a THz absorber. Gray, light blue, and black areas represent the surface impedance boundary condition (SIBC) imposed by the partially reflecting sheet (PRS), the dielectric, and the metal sheet, respectively. The inset shows the possible implementation of the PRS unit cell through a metal strip grating. (b) Equivalent transmission-line model of the device.

Since the PRS is fully characterized by an SIBC, the overall FPCR can be described through a transverse equivalent network (TEN). The latter is constituted by a short-circuited transmission-line segment (characteristic admittance Y_d and propagation constant k_{zd}) of length h (height of the dielectric slab with relative permittivity $\varepsilon_r = \varepsilon_r' - j\varepsilon_r''$) shunted by the PRS Y_s admittance and terminated on the vacuum characteristic admittance Y_0 (see Fig. 1(b)). As a consequence, the reflection coefficient r of an incident plane wave is immediately found and reads:

$$r = \frac{Y_0 - jB_s + jY_d \cot(k_{zd}h)}{Y_0 + jB_s - jY_d \cot(k_{zd}h)}. \tag{1}$$

It is worth noting that the denominator in (1) corresponds to the dispersion equation of an FPCR acting as a leaky-wave antenna (see, e.g., [27] and references therein). By considering a dipole-like source embedded in the cavity, FPCRs have been widely used as two-dimensional (2-D) quasi-uniform leaky-wave radiators [28]. Interestingly, by exploiting a ray-optics approximation (or the reciprocity theorem [29]), it is possible to evaluate the power radiated at broadside. The latter is inversely proportional to the square of the absolute value of

the reflection-coefficient denominator in (1) [30]:

$$P_0 \propto |Y_0 + jB_s - jY_d \cot(k_{zd}h)|^{-2}. \quad (2)$$

As a result, the complex poles of (1) also correspond to the complex poles of (2), thus the resonance conditions of the FPCR when a THz beam impinges at normal incidence (the approach can be generalized for any incident angle), are identical to the condition for maximum radiated power at broadside. In this context, as shown in [29], the optimum cavity height for the FPCR leaky-wave antenna can be found by taking the real part of these complex poles:

$$h_{\rm opt}^{\rm LW} = \frac{c_0}{2f_0\sqrt{\varepsilon_r'}}\left\{m + \frac{1}{\pi}\mathrm{Re}\left[\mathrm{acot}\left(\frac{B_s\eta_0 - j}{\sqrt{\varepsilon_r}}\right)\right]\right\} \quad (3)$$

with $\eta_0 \simeq 120\ \Omega$, c_0, and m being the vacuum characteristic impedance, the speed of light in vacuum, and the resonance order of the FPCR, respectively. Interestingly, under the assumption of low losses and highly reflective PRS (viz., $|B_s|\eta_0 \gg 1$ or, equivalently, $|X_s| \ll \eta_0$), it is possible to approximate (3) as in equation (32) of [31]:

$$h_{\rm opt}^{\rm LW} \simeq \frac{c_0}{2f_0\sqrt{\varepsilon_r'}}\left(m + \frac{\sqrt{\varepsilon_r'}}{\pi\eta_0 B_s}\right). \quad (4)$$

Under the same assumptions, it is also possible to find an analytical approximation of the power radiated at broadside in (2) where the optimum cavity height in (3) is considered:

$$P_0 \propto \left|(Y_0 + jB_s)(-\frac{\sqrt{\varepsilon_r}}{B_s\eta_0} + j\pi\frac{\tan\delta}{2}) + jY_d\right|^{-2} \quad (5)$$

with $\tan\delta = \varepsilon_r''/\varepsilon_r'$ being the dielectric loss tangent.

At this point, by exploiting a similar leaky-wave approach to that used for describing the FPCR as an antenna, it is possible to find an original theoretical framework for using such a device as an absorber. In particular, if the metal back plate of the FPCR is thicker than the skin depth—so as to completely prevent the leakage of incident wave beyond the FPCR ground plane [5]—all the power which is not reflected from the FPCR is absorbed. As a consequence, a simple formula of the absorptance A can be obtained as follows:

$$A = 1 - |r|^2. \quad (6)$$

By substituting (1) in (6) is thus possible to analytically evaluate the absorptance of an FPCR as a function of the working frequency, PRS sheet admittance, and cavity height. Therefore, thanks to the simplicity of its structure and the powerful theoretical framework discussed so far, it is possible to design a critical absorber at almost any frequency with simple and low-cost materials. Specifically, the optimum cavity height $h_{\rm opt}$ for maximum absorptance at normal incidence (the approach can be generalized for any incident angle) can easily be expressed analytically as a function of f_0 and B_s by equating to zero the numerator in (1):

$$h_{\rm opt} = \frac{c_0}{2f_0\sqrt{\varepsilon_r'}}\left\{m + \frac{1}{\pi}\mathrm{Re}\left[\mathrm{acot}\left(\frac{B_s\eta_0 + j}{\sqrt{\varepsilon_r}}\right)\right]\right\}. \quad (7)$$

Interestingly, such a condition converges to (4) for low losses and highly reflective PRS indicating that, in these working situations, the condition for the maximum power radiated at broadside corresponds to that of the maximum absorptance. With these assumptions, using (7) in (6), it is also possible to find the following analytical formula for the absorptance profile as a function of the PRS susceptance B_s:

$$A \simeq \frac{2Y_0^2\pi\sqrt{\varepsilon_r}\tan\delta}{\left|(Y_0 + jB_s)(-\frac{\sqrt{\varepsilon_r}}{B_s\eta_0} + j\pi\frac{\tan\delta}{2}) + jY_d\right|^2} \quad (8)$$

where it is noted that (8) and (5) have the same denominator, thus the same dependence from B_s or, equivalently, X_s. This is a consequence of the reciprocity theorem under the abovementioned conditions, as thoroughly discussed next.

At this point, it is possible to find a design equation for the optimum sheet reactance $X_s^{\rm opt}$ value for a normal-incidence FPCR absorber by analytically seeking for the maximum of (8). After a few mathematical steps, this procedure leads to:

$$|X_s^{\rm opt}| = \eta_0\sqrt{\frac{\pi\tan\delta}{2\sqrt{\varepsilon_r}}}. \quad (9)$$

Since (9) is found under the assumptions of (8) (viz., a low-loss substrate and a highly reflective PRS), the latter corresponds to the formula for the optimum susceptance value in equation (23) of [30] for achieving the maximum radiated power at broadside in an FPCR working as a leaky-wave antenna. Interestingly, (9) also corresponds to the desired *critical-absorption* condition for highly reflective PRS. This aspect can be easily demonstrated by equating, for $B_s\eta_0 \gg 1$ and $\mu_r = 1$, the dielectric loss tangent $\tan\delta$ to the equivalent loss tangent of radiative losses reported in [32], viz.:

$$\tan\delta_{\rm rad} = \frac{2}{\pi}\sqrt{\frac{\varepsilon_r}{\mu_r}}\frac{1}{(B_s\eta_0)^2 + 1}. \quad (10)$$

The design workflow of FPCR absorbers is thus clear: through a simple transmission-line model, it directly links the desired operating frequency to the required substrate electrical thickness and to the PRS equivalent sheet reactance X_s. Consequently, to design an absorber operating at a target frequency f_0 using a dielectric slab with known relative permittivity ε_r and loss tangent $\tan\delta$, formula (9) can be employed to determine the optimal value $X_s^{\rm opt}$ and, then, expression (7) is used to find $h_{\rm opt}$. At this stage, the unit-cell geometry required to achieve the desired sheet reactance can be obtained either through approximate analytical expressions [26] or through accurate full-wave simulations [24] (as thoroughly discussed in Section III). Starting from this initial structure, the design process can then be finalized by numerically optimizing (6), while accounting for the dispersive behavior of both the substrate material and the homogenized PRS response.

At this point, to confirm the validity of the proposed theoretical framework and show the limits of its approximations, a few case studies are numerically investigated in the following subsection.

B. Numerical Results

The main objective of this subsection is to analytically retrieve, at the resonance frequency of $f_0 = 300$ GHz, the

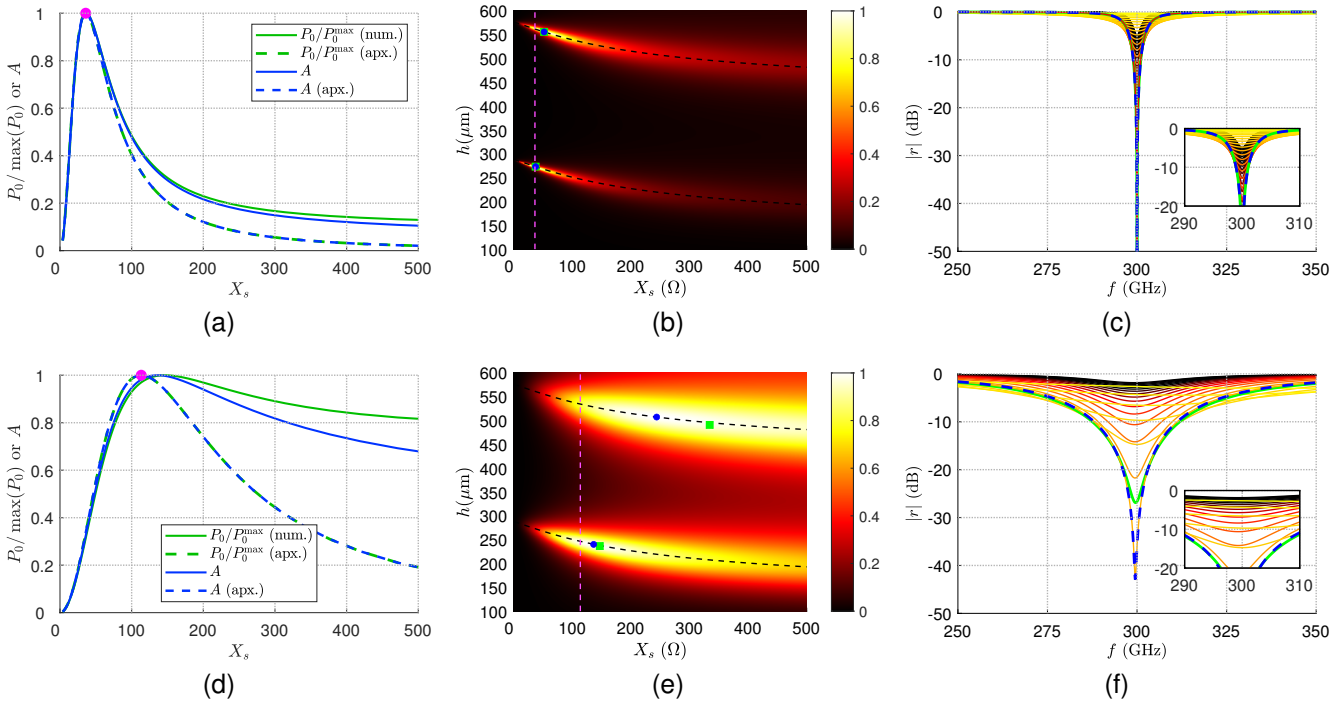

Fig. 2. Theoretical results for the design of critical absorbers at $f_0 = 300$ GHz based on Fabry–Perot cavity resonators realized through a grounded dielectric slab with relative permittivity $\varepsilon_r' = 3$ and loss tangent $\tan\delta = 0.01$ (first row) or $\tan\delta = 0.1$ (second row). Absorptance A and maximum power radiated at broadside P_0 as a function of the sheet reactance X_s when the optimum cavity height in (7) is assumed for a dielectric substrate with (a) $\tan\delta = 0.01$ and (d) $\tan\delta = 0.1$. The condition of the optimum reactance sheet value (9) is reported through a magenta marker. Color maps of the absorptance as a function of the cavity height h and the PRS reactance X_s for a Fabry–Perot cavity absorber working at $f_0 = 300$ GHz with a dielectric loss tangent of (b) $\tan\delta = 0.01$ and (e) $\tan\delta = 0.1$: while the optimum h and X_s values obtained by means of (7) and (9) are reported through black and magenta dashed lines, respectively, the blue dots and the green squares indicate the numerically computed conditions for the best absorptance and the maximum power radiated at broadside for each resonance order m, respectively. Absolute value of the reflection coefficient of an absorber with (c) $\tan\delta = 0.01$ or (f) $\tan\delta = 0.1$ designed to resonate at $f_0 = 300$ GHz with the optimum cavity height h in (7) computed for different X_s values (while colors shade from black to red and yellow as $X_s \to 0$, the blue and green lines indicate the condition for the maximum absorptance and the maximum power radiated at broadside, respectively).

absorptance and the power radiated at broadside of two FPCRs based on two case-study materials with two different loss tangent—$\tan\delta_1 = 0.01$ and $\tan\delta_2 = 0.1$—and the same relative permittivity $\varepsilon_r' = 3$. These two cases are representatives of a moderately low-loss and moderately high-loss material.

The absorptance A (given by (6)) and radiated power at broadside P_0 (given by (2)) are initially obtained assuming the optimum cavity height for the first, nonzero, resonance (viz., $m = 1$)—given by (7)—and shown, normalized with respect to their maxima, in Fig. 2 as a function of the sheet reactance X_s. As expected, the normalized A and P_0 are almost identical for moderately low losses (see Fig. 2(a)) and show only minor differences for moderately high losses (see Fig. 2(d)). Interestingly, the critical absorption is reached for smaller X_s values when the loss tangent is $\tan\delta = 0.01$ (Fig. 2(a)) rather than $\tan\delta = 0.1$ (Fig. 2(d)). This effect is a direct consequence of (9): a lower loss tangent calls for a lower sheet reactance. In physical terms, a lower dissipation of power into the dielectric material has to be balanced by a lower leakage rate of radiated power, which is obtained by increasing the reflectivity of the PRS, thus by decreasing its sheet reactance. In this context, it is worthwhile to point out that dielectric losses are commonly the main dissipative mechanism at low-THz frequencies since they are one order higher than the ohmic losses [6]. Still, by observing Fig. 2(a) and (d), it is also interesting to note how the approximate expression for the maximum radiated power at broadside (5) and that for the absorptance (8) are more accurate, as theoretically expected, for low-loss materials and highly reflective PRSs. Under the same conditions, the validity of the PRS design equation (9) is also confirmed since it corresponds to the magenta marker in Figs. 2(a) and (d). The latter is placed exactly at, or in close proximity of the maximum absorptance level for the $\tan\delta_1$ or $\tan\delta_2$ case, respectively. In any case, it is worth noting that the effectiveness of the leaky-wave approach [28] and of the proposed approximations becomes limited as the PRS reflectivity decreases, as corroborated by the disagreements among the curves in Figs. 2(a) and (d) as X_s increases.

At this point, thanks to the theoretical approach presented in Sec. II.A, it is also possible to evaluate the absorptance of FPCRs based on these two materials when the condition of the optimum cavity height in (7) is not necessarily satisfied. To do so, (6) is computed at $f_0 = 300$ GHz as a function of both the PRS reactance $X_s = -1/B_s$ and the cavity height h. The obtained results are reported for $\tan\delta = 0.01$ and $\tan\delta = 0.1$ in Figs. 2(b) and (e), respectively, and show interesting outcomes. First, the validity of equation (7) (indicated through two dashed black lines for $m = 1$ and $m = 2$) which reports the optimum cavity height as a function of X_s is clearly confirmed in these figures since the latter always fall in the

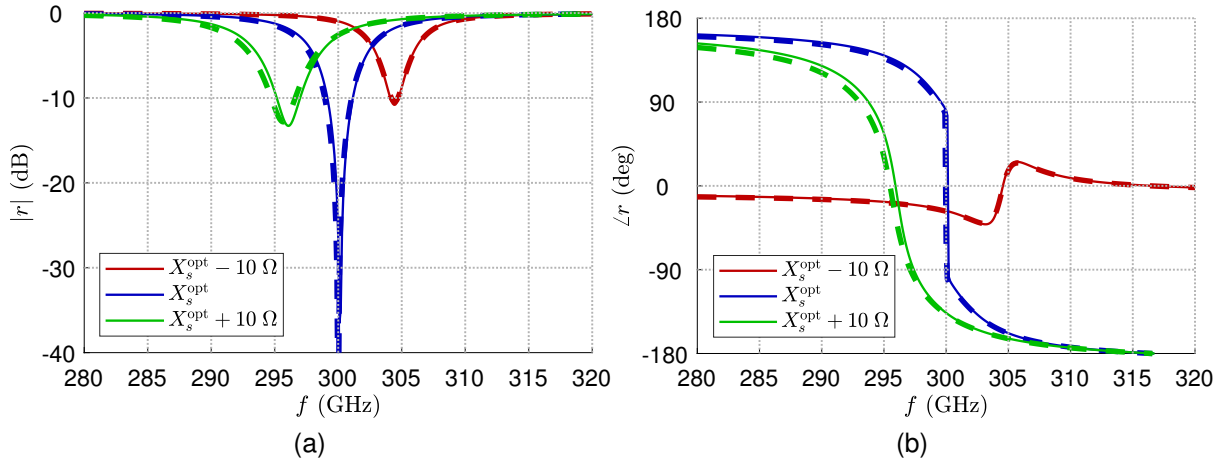

Fig. 3. (a) Magnitude and (b) phase of the reflection coefficient of the designed critical-absorption Fabry–Perot cavity resonator based on a grounded dielectric slab with $\varepsilon_r' = 3$ and $\tan\delta = 0.01$ (blue curves). Simulation and theoretical results obtained by means of the equivalent transmission-line model of the device are reported through solid and dashed lines, respectively. The green/red curve indicates the reflectance spectrum for an overcoupled/undercoupled case obtained through a PRS with a sheet reactance larger/smaller of $10\,\Omega$ with respect to the optimum $X_s^{\rm opt}$ value.

region where the absorptance is maximized. Second, for each resonance order, the optimal operating points of the FPCRs used as leaky-wave antennas to radiate maximum power at broadside (green squares, numerically evaluated through (2)) have been identified. For moderately low-loss dielectric slabs, these points coincide with the critical-absorption points (blue dots, obtained from (6)), which correspond to the condition where the radiation leakage rate equals the dielectric absorption rate. Conversely, for high-loss dielectrics, the two sets of points do not coincide. Interestingly, the optimized values of the cavity height computed through (7) (black dashed lines) correspond to the best working points in terms of both power radiated at broadside for the leaky-wave-antenna configuration and the absorptance for the FPCR absorber. This is due to the fact that (7) corresponds to the design formula (4) for Fabry–Perot cavity antennas pointing at broadside when highly reflective PRS are considered (viz., when $B_s\eta_0 \gg 1$). Still, (7) clearly holds regardless of the m value demonstrating that the critical absorption can be reached with any resonance order inside the FPCR since the working principle of the device is not based on the specific design of the PRS or the choice of the substrate height, but on their comprehensive response, irrespective of the order of the resonance. Even more interestingly, Fig. 2(b) demonstrates that the design formulas of the optimum cavity height (7) and sheet reactance (dashed magenta line obtained through (9)) perfectly work under their operating conditions of relatively low-loss materials and highly reflective PRSs. Moreover, although (9) does not provide the optimum design parameters for the $\tan\delta_2$ case, Fig. 2(e) shows that for higher losses, the near-optimal region is larger, thus giving more tolerance to the choice of X_s and h.

This aspect is related to the lower quality factor Q of FPCRs based on high-loss dielectrics. To corroborate this point, Figs. 2(c) and (f) report—for the $\tan\delta = 0.01$ and $\tan\delta = 0.1$ cases, respectively—the reflection coefficient computed through (1) by assuming, for different X_s values (colors shade from black to red and yellow as $X_s \to 0$), the choice of the optimum cavity height h. Despite the level of the dip (which depends on the absorption level related to the X_s value, as shown in Figs. 2(b) and (e)), FPCRs based on materials with higher losses have a larger bandwidth with a high absorption rate. As a consequence, for high-loss materials, it is possible to achieve a large absorption rate also without the optimum h value for the considered design frequency (see the difference between Figs. 2(b) and (e) with $\tan\delta = 0.01$ and $\tan\delta = 0.1$, respectively). Remarkably, in Figs. 2(c) and (f), it is also possible to appreciate the differences between the optimum designs for radiating power at broadside (green solid line) or absorbing the THz signal (blue dashed line) depending on the losses. This is due to the fact that, for low-loss materials (see Fig. 2(c)), almost all power trapped in the FPCR coming from an orthogonally incident THz wave corresponds, by virtue of the reciprocity theorem, to the power radiated at broadside by the same device working as a leaky-wave transmitter [24]. On the contrary, when dielectric slabs with high $\tan\delta$ values are considered (see Fig. 2(f)), an important contribution to the absorption rate is directly given by the dielectric losses. As a consequence, the best condition for radiating at broadside through non-efficient (due to the high losses [32]) FPCR antennas does not exactly correspond to the best design for FPCR absorbers. This conclusion is corroborated in Fig. 2(f) by the clear difference between the green and the blue lines (they almost coincide, instead, for the low-loss case in Fig. 2(c)).

To corroborate these purely analytical results, the full-wave simulation of the maximum-absorptance design for a dielectric with $\varepsilon_r' = 3$ and $\tan\delta = 0.01$ has been conducted on CST Microwave Studio [33]. Specifically, a critical-absorber FPCR has been designed through the proposed approach by obtaining an optimum cavity height of $h_{\rm opt} = 273.17$ µm and a sheet reactance of $X_s^{\rm opt} = 37.037\ \Omega$. The latter is implemented on the full-wave-solver periodic environment through a grounded dielectric slab with an SIBC on top which can be designed, as in [28], through a transparent impedance

boundary condition with a linearly dispersive frequency behavior. The obtained results are reported through a blue color in Fig. 3 confirming the validity of the proposed theoretical method due to the impressive agreement of the phase and magnitude profile of the reflection coefficient computed by means of full-wave simulations (solid lines) and the transmission-line model (dashed lines). Interestingly, the critical-absorption condition is also confirmed due to the very low absolute value of the reflection coefficient at the working frequency of $f_0 = 300$ GHz and the step-like profile of its phase. As a comparison, the reflectance spectrum of two additional cases constituted by the same device with a different PRS are also reported in Fig. 3. Specifically, with $X_s = X_s^{\text{opt}} + 10\ \Omega$ and $X_s = X_s^{\text{opt}} - 10\ \Omega$, a much lower absorptance level (the magnitude of the reflectance is about -10 dB instead of -40 dB) and a smoother phase profile representing a overcoupled and an undercoupled resonator (rather than the critical-absorption, step-like curve) are obtained, respectively. It is thus clear that the X_s^{opt} value for which the maximum absorptance occurs in Fig. 2(a) and (d) not only corresponds to the critical-absorption condition, but also divides the operating principle of the FPCR as an absorber into two distinct regions depending on the X_s value, i.e., the undercoupled regime ($X_s < X_s^{\text{opt}}$) and the overcoupled regime ($X_s > X_s^{\text{opt}}$).

As a conclusion for this Sec. II, one can infer that FPCRs can be efficiently exploited as absorbers at THz frequencies by properly choosing the design parameters of the device as a function of the available material. To achieve an (almost) critical absorption, the loss level of the latter has to be chosen as a compromise between the robustness of the device to fabrication tolerances (high losses permit a large quality factor of the resonator achieving a good absorption rate even with nonexact cavity heights and PRS designs) and selectivity in frequency (low-loss materials could lead to an ultra-narrowband absorber). A good compromise is given by FR4 materials, as experimentally demonstrated next.

III. Design, Fabrication, and Experiment

In this Sec. III, the design, fabrication process, and experimental validation of an FPCR-based critical absorber at THz frequencies are reported in the following three distinguished subsections, respectively.

A. Material Characterization and Metasurface Design

With the aim of realizing a THz absorber, the first step for the correct design of the device is related to the characterization of the target dielectric material. As abovementioned, an FR4 dielectric substrate could present a good compromise of losses in terms of fabrication tolerances and frequency selectivity since such microwave-target substrates show increased losses at THz [34]. To confirm this aspect, due to the absence of information in the material datasheet at these frequencies, the dielectric features of an ISOLA370HR sample has been measured in the THz band through a TDS setup mounted in reflection mode. The characterization was performed through the procedure presented in [34]: first the signal of a metallic reference plane was collected and then used to normalize the

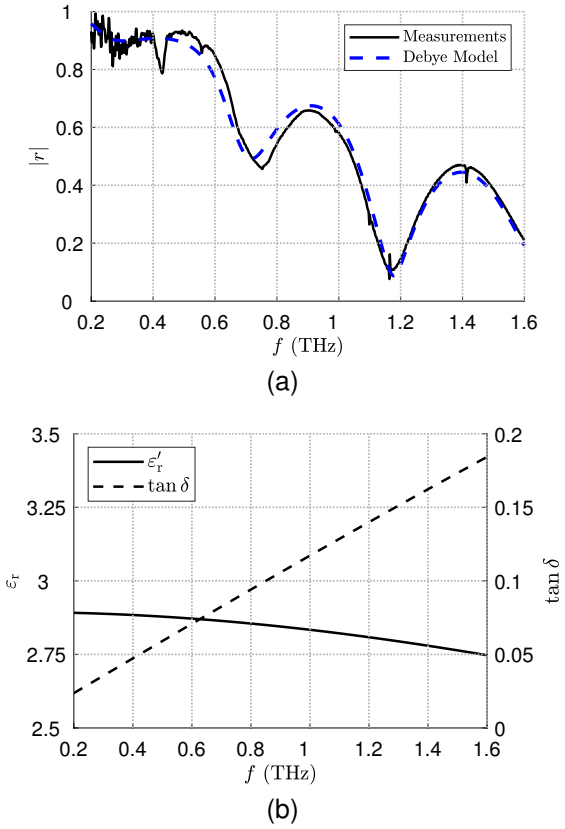

Fig. 4. (a) Measured (black solid line) and numerical (blue dashed line) reflection coefficient of the considered grounded FR4 slab characterized through a Debye model. (b) Real part of the dielectric permittivity (black solid line) and loss tangent (black dashed line) of the proposed Debye model representing the ISOLA370 material at THz frequencies.

spectrum in presence of the device under test (DUT), viz., the grounded ISOLA370HR slab. By exploiting the data post-processing paradigm in [34], the DUT thickness $h = 192$ μm and dielectric properties were calculated. Specifically, by means of a simple transmission-line model of the DUT, the grounded dielectric slab was characterized by fitting the parameters of a Debye model representing the device (further information can be found in [34]). The obtained results are reported in Fig. 4. More precisely, in Fig. 4(a) we show the agreement between measured results (black solid line) and the transmission-line model considering the DUT described by the abovementioned Debye model; Fig. 4(b) reports, instead, the real part of the permittivity (solid line) and the loss tangent (dashed line) of the ISOLA370HR sample under test in the THz frequency range. A $\tan\delta \simeq 0.048$ is found around the desired working frequency of 400 GHz (chosen in accordance to the slab thickness) with a real part of the relative permittivity of $\varepsilon_r' \simeq 2.88$.

Once the features of the dielectric substrate are known, the design of the PRS unit cell is needed. Specifically, with the idea of exploiting the homogenization formulas in [26], a metal strip grating is considered in this work (see the inset in Fig. 1(a)). In this context, it is crucial to note the need of taking into account an additional thin layer of polyimide in the design procedure. The latter is necessary to planarize the dielectric substrate before fabricating the patterned metallic

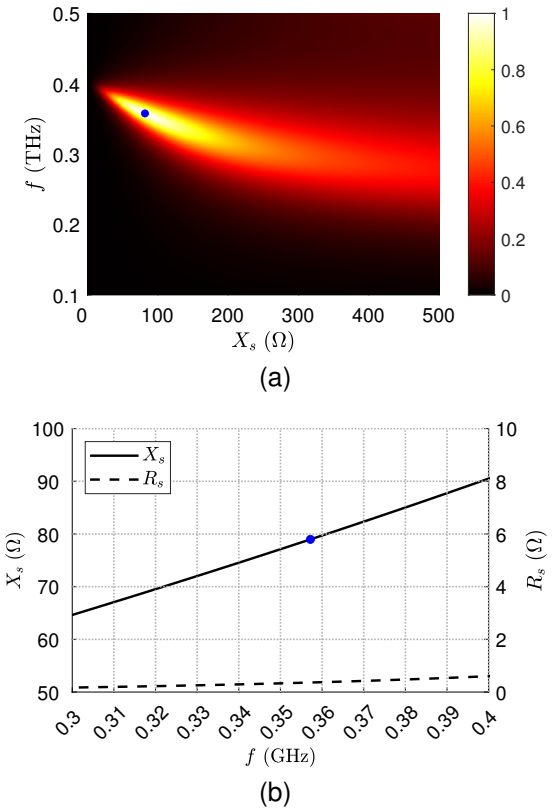

Fig. 5. (a) Absorptance as a function of the PRS sheet reactance X_s and the resonance frequency f when a ISOLA370HR substrate, described through the Debye model in Fig. 4, is considered with a thickness $h = 217$ μm. (b) Real (dashed line) and imaginary (solid line) part of the sheet impedance $Z_s = R_s + jX_s$ of the homogenized metasurface constituted by a metal strip grating with period $p = 200$ µm and strip width $w = 51$ µm (see Fig. 1 for the definition of the geometrical parameters).

sheet (this point is thoroughly discussed next in Sec. III.B). This material presents very similar dielectric features and losses to the ISOLA370HR substrate at THz frequencies (see, e.g., [35]). As a consequence, one has to simply consider an *effective* thickness of the substrate to design the device, $h = 217$ µm in this case. Once the cavity height is known, it is possible to exploit the design procedure presented in Sec. II to retrieve, as a function of the surface reactance sheet X_s and the working frequency f, the absorption rate of an FPCR based on the ISOLA370HR characterized as in Fig. 4. The results of this analysis are reported in Fig. 5(a) where the critical-absorption condition, indicated by a light-blue dot, is given at the working frequency of $f_0 = 357$ GHz through a sheet reactance of $X_s \simeq 80$ Ω. (It is worth noting that a frequency shift with respect to the abovementioned 400-GHz resonance is due to the different effective cavity height which considers the additional polymide layer.) According to the formulas in [26], the desired X_s value can be realized through a metal strip grating with periodicity $p = 200$ µm and strip width $w = 51$ µm. This aspect has been corroborated through full-wave simulations of the real structure. Specifically, the Z_s value of an aluminum strip grating has been computed through the numerical computation of the reflection coefficient given by such a metasurface printed on top of a grounded slab [28] with the dielectric characteristics in Fig. 4 directly

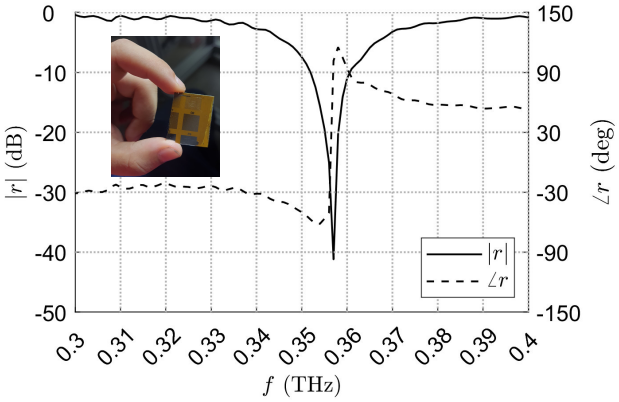

Fig. 6. Absolute value (solid line) and phase (dashed line) of the measured reflection coefficient generated by the designed critical absorber based on a Fabry–Perot cavity resonator. The insets shows the device picture.

imported in the CST, frequency-domain, full-wave solver [33]. These results are shown in Fig. 5(b) where Z_s is reported as a function of the frequency f. Interestingly, although much lower and negligible with respect to the target X_s at f_0, there is a nonzero value of the sheet resistance R_s due to the realistic metasurface losses.

B. Fabrication Process

A 192-µm-thick ISOLA370HR FR4 double-sided board was used as the substrate. To protect one copper surface, a dry-film photoresist (Ordyl FP400, Elga Europe) was laminated, and the opposite copper side was completely etched in a 35 wt% ferric chloride ($FeCl_3$) solution. The exposed surface was then planarized by spin-coating a polyimide layer (PI2611, HD Microsystems), which was subsequently cured in a nitrogen atmosphere at 250 °C for 2 hours. The sample was then loaded into an evaporator, and a 250 nm-thick aluminum film was deposited. Photolithographic patterning of the grid (50 × 50 unit cells) was carried out using a positive resist (MICROPOSIT S1813). The aluminum layer was selectively etched for 12 minutes in a mixed acid solution containing nitric acid (HNO_3), phosphoric acid (H_3PO_4), acetic acid (CH_3COOH), and water. After removing the residual resist in acetone, the protective dry-film layer on the opposite side was stripped using an alkaline solution (Ordyl Stripper 5600). Finally, the sample was rinsed with deionized water and dried under a nitrogen flow.

C. Experimental Validation

To experimentally validate the device, the sample is placed on the reference metal plane of the THz TDS mounted in reflection mode, as in [25]. In this manner, the absorber is under the THz beam generated by the measurement setup and focused in a spotsize of about $1\,\mathrm{mm}$ [36]. In this context, it is worth nothing that such a beam collects the response of the FPCR only (i.e., with negligible edge effects) thanks to the relatively large metasurface area (viz., as shown in the inset of Fig. 6, a square of $1\ \mathrm{cm}^2$ which corresponds to a $11.9\lambda_0 \times 11.9\lambda_0$ surface at the absorber working frequency).

As concerns the measurement process, a similar procedure to that used for characterizing the material substrate has been carried out. First, a reference trace has been collected without the absorber on the metallic plate. Then, by properly placing the center of the absorber on the center of the THz focused beam, the reflection coefficient is achieved through the normalization of the measured signal with respect to the reference one.

Measurement results, which are reported in Fig. 6, clearly demonstrate the effectiveness of the proposed absorber. The device is indeed capable of reaching, for the reflection coefficient r, an impressive absolute value of -40 dB at the expected working frequency $f_0 = 357$ GHz with a relatively high selectivity level (please note the different x-axis scales in Fig. 2(c) and (f) with respect to that in Fig. 6). Even more interestingly, the condition of almost perfect critical absorption is confirmed in Fig. 6 by the phase profile of the reflection coefficient since, as theoretically expected for critical absorbers (see, e.g., [8] and Fig. 3), $\angle r$ is almost vertical at the resonance frequency f_0. In this context, it is worthwhile to point out that there is not a perfect step-like phase profile as expected by the critical-absorption condition [13], but the DUT presents a slightly undercoupled behavior. This aspect is mainly due to the approximate characterization of the polymide layer and due to the quasi-normal incidence of the THz beam on the FCPR. The TeraFlash Pro setup [36] used in this work presents in fact a transverse-electric (TE) polarized THz beam which impinges with an incident angle $\theta_i = 8^\circ$ instead of a normal incidence (as assumed in this paper so far). In any case, the reflectance phase curve is almost vertical (as a reference, observe the much more oblique phase profile when a shift of 10 Ω is present in Fig. 3(b)) and the reflection coefficient tends to zero in modulus (-40 dB), experimentally confirming the validity of the proposed approach for designing FPCR absorbers in the THz range.

IV. Conclusion

The theoretical analysis, design workflow, and experimental validation of innovative THz absorbers based on a Fabry–Perot cavity resonator are presented in this work. By originally exploiting a leaky-wave paradigm for designing critical absorbers, analytical formulas for the absorptance and the best cavity height of the device have been found based on a transmission-line-model analysis. The theoretical design of the device has then been corroborated through numerical analyses, full-wave simulations, and experimental validations based on THz time-domain spectroscopy in reflection mode. Obtained results demonstrate that Fabry–Perot cavity resonators are a promising candidate for achieving a THz ultra-narrowband critical absorption with the simultaneous advantages of having a relatively simple structure and of presenting different degrees of freedom in terms of materials and metasurface typologies. Potential solutions to increase the operating bandwidth and angular stability for applications requiring broadband absorption and/or low angular dispersion could be explored in future research, such as employing innovative configurations based on thick partially reflecting sheets or incorporating tunable elements into the homogenized-metasurface design. Conversely, an even more narrowband and highly selective absorber for sharp-filtering applications can be achieved by using a highly reflective homogenized metasurface combined with a low-loss dielectric substrate.

References

[1] A. Rämer, E. Negri, E. Dischke, S. Chevtchenko, H. Yazdani, L. Schellhase, V. Krozer, and W. Heinrich, "Monolithically integrated THz detectors based on high-electron-mobility transistors," *Sensors*, vol. 25, no. 11, May 2025.

[2] G. Valušis, A. Lisauskas, H. Yuan, W. Knap, and H. G. Roskos, "Roadmap of terahertz imaging 2021," *Sensors*, vol. 21, no. 12, p. 4092, Jun. 2021.

[3] T. Kürner, D. M. Mittleman, and T. Nagatsuma, "Thz communications: Paving the way towards wireless Tbps," *Springer Ser. Opt. Sci.*, vol. 234, 2016.

[4] S. Venkatachalam, K. Zeranska-Chudek, M. Zdrojek, and D. Hourlier, "Carbon-based terahertz absorbers: Materials, applications, and perspectives," *Nano Select*, vol. 1, no. 5, pp. 471–490, Jul. 2020.

[5] C. Chen, M. Chai, M. Jin, and T. He, "Terahertz metamaterial absorbers," *Adv. Mat. Techn.*, vol. 7, no. 5, p. 2101171, Dec. 2021.

[6] H. Tao, N. I. Landy, C. M. Bingham, X. Zhang, R. D. Averitt, and W. J. Padilla, "A metamaterial absorber for the terahertz regime: design, fabrication and characterization," *Optics express*, vol. 16, no. 10, pp. 7181–7188, May 2008.

[7] H. Tao, C. Bingham, A. Strikwerda, D. Pilon, D. Shrekenhamer, N. Landy, K. Fan, X. Zhang, W. Padilla, and R. Averitt, "Highly flexible wide angle of incidence terahertz metamaterial absorber: Design, fabrication, and characterization," *Physical Review B—Condensed Matter and Materials Physics*, vol. 78, no. 24, p. 241103, Dec. 2008.

[8] D. C. Zografopoulos, I. Dionisiev, N. Minev, G. Petrone, F. Maita, L. Maiolo, D. Dimitrov, V. Marinova, A. Liscio, V. Mussi *et al.*, "Terahertz time-domain characterization of thin conducting films in reflection mode," *IEEE Trans. Antennas Propag.*, vol. 72, no. 12, pp. 9301–9316, Dec. 2024.

[9] J. R. Piper, V. Liu, and S. Fan, "Total absorption by degenerate critical coupling," *Appl. Phys. Lett.*, vol. 104, no. 25, Jun. 2014.

[10] Y. Ra'di, C. R. Simovski, and S. A. Tretyakov, "Thin perfect absorbers for electromagnetic waves: theory, design, and realizations," *Phys. Rev. Appl.*, vol. 3, no. 3, p. 037001, Mar. 2015.

[11] S. Xiao, X. Wang, J. Duan, T. Liu, and T. Yu, "Engineering light absorption at critical coupling via bound states in the continuum," *J. Opt. Soc. America B*, vol. 38, no. 4, pp. 1325–1330, Apr. 2021.

[12] X. Long, J. Bai, Y. Zhang, M. Zhu, X. Guo, J. Wang, W. Wang, and R. Lou, "Polarization-independent perfect absorption in monolayer black phosphorus metasurfaces at terahertz frequencies via critical coupling," *ACS Omega*, vol. 9, no. 32, pp. 35 052–35 059, Aug. 2024.

[13] G. Isić, B. Vasić, D. C. Zografopoulos, R. Beccherelli, and R. c. v. Gajić, "Electrically tunable critically coupled terahertz metamaterial absorber based on nematic liquid crystals," *Phys. Rev. Appl.*, vol. 3, p. 064007, Jun. 2015.

[14] G. Isić, G. Sinatkas, D. C. Zografopoulos, B. Vasić, A. Ferraro, R. Beccherelli, E. E. Kriezis, and M. Belić, "Electrically tunable metal–semiconductor–metal terahertz metasurface modulators," *IEEE J. Sel. Top. Quantum Electron.*, vol. 25, no. 3, pp. 1–8, Jan. 2019.

[15] J. R. Tischler, M. S. Bradley, and V. Bulović, "Critically coupled resonators in vertical geometry using a planar mirror and a 5 nm thick absorbing film," *Opt. lett.*, vol. 31, no. 13, pp. 2045–2047, Apr. 2006.

[16] H. Li, M. Qin, L. Wang, X. Zhai, R. Ren, and J. Hu, "Total absorption of light in monolayer transition-metal dichalcogenides by critical coupling," *Opt. Express*, vol. 25, no. 25, pp. 31 612–31 621, Dec. 2017.

[17] F. Costa and A. Monorchio, "Multiband electromagnetic wave absorber based on reactive impedance ground planes," *IET Microw., Antennas Propag.*, vol. 4, no. 11, pp. 1720–1727, Nov. 2010.

[18] S. Thongrattanasiri, F. H. Koppens, and F. J. García de Abajo, "Complete optical absorption in periodically patterned graphene," *Phys. rev. lett.*, vol. 108, no. 4, p. 047401, Jan. 2012.

[19] S. Guo, J. Deng, J. Zhou, Y. Yu, Y. Bu, T. Zhu, X. Ren, Z. Li, W. Lu, and X. Chen, "Combined role of polarization matching and critical coupling in enhanced absorption of 2d materials based on metamaterials," *Opt. Express*, vol. 29, no. 6, pp. 9269–9282, Mar 2021.

[20] H. Haus, *Waves and Fields in Optoelectronics*, ser. Prentice-Hall series in solid state physical electronics. Prentice-Hall, 1984.

[21] F. Costa, S. Genovesi, A. Monorchio, and G. Manara, "A circuit-based model for the interpretation of perfect metamaterial absorbers," *IEEE Trans. Antennas Propag.*, vol. 61, no. 3, pp. 1201–1209, Mar. 2013.
[22] S. Tretyakov, *Analytical Modeling in Applied Electromagnetics*. Norwood, MA, USA: Artech House, 2003.
[23] W. Fuscaldo, S. Tofani, D. C. Zografopoulos, P. Baccarelli, P. Burghignoli, R. Beccherelli, and A. Galli, "Systematic design of THz leaky-wave antennas based on homogenized metasurfaces," *IEEE Trans. Antennas Propag.*, vol. 66, no. 3, pp. 1169–1178, Mar. 2018.
[24] W. Fuscaldo, F. Maita, L. Maiolo, R. Beccherelli, and D. C. Zografopoulos, "Broadband terahertz characterization and electromagnetic models for fishnet metasurfaces: From the homogenization to the resonant regime," *IEEE Trans. Antennas Propag.*, Aug. 2024.
[25] W. Fuscaldo, E. Negri, F. Maita, L. Maiolo, R. Beccherelli, and D. C. Zografopoulos, "Modal and reflective properties of capacitive and inductive terahertz metasurfaces," *Adv. Opt. Mat.*, p. e01605, 2025, Early Access.
[26] O. Luukkonen, C. Simovski, G. Granet, G. Goussetis, D. Lioubtchenko, A. V. Raisanen, and S. A. Tretyakov, "Simple and accurate analytical model of planar grids and high-impedance surfaces comprising metal strips or patches," *IEEE Trans. Antennas Propag.*, vol. 56, no. 6, pp. 1624–1632, Jun. 2008.
[27] P. Burghignoli, W. Fuscaldo, and A. Galli, "Fabry–Perot cavity antennas: The leaky-wave perspective," *IEEE Antennas Propag. Mag.*, vol. 63, no. 4, pp. 116–145, Aug. 2021.
[28] E. Negri, W. Fuscaldo, P. Burghignoli, and A. Galli, "An overview of design techniques for two-dimensional leaky-wave antennas," *Appl. Sci.*, vol. 15, no. 4, p. 1854, Feb. 2025.
[29] W. Fuscaldo, D. R. Jackson, and A. Galli, "Optimum cavity height for radiating a pencil beam at broadside from a fabry–perot cavity antenna," *IEEE Antennas Wireless Propag. Lett.*, vol. 24, no. 8, pp. 2222–2226, Apr. 2025.
[30] G. Lovat, P. Burghignoli, and D. R. Jackson, "Fundamental properties and optimization of broadside radiation from uniform leaky-wave antennas," *IEEE Trans. Antennas Propag.*, vol. 54, no. 5, pp. 1442–1452, May 2006.
[31] T. Zhao, D. Jackson, J. Williams, and A. Oliner, "General formulas for 2-D leaky-wave antennas," *IEEE Trans. Antennas Propag.*, vol. 53, no. 11, pp. 3525–3533, Nov. 2005.
[32] W. Fuscaldo, "Rigorous evaluation of losses in uniform leaky-wave antennas," *IEEE Trans. Antennas Propag.*, vol. 68, no. 2, pp. 643–655, Feb. 2020.
[33] "CST products Dassault Systèmes, France, 2021." [Online]. Available: http://www.cst.com
[34] W. Fuscaldo, F. Maita, L. Maiolo, R. Beccherelli, and D. C. Zografopoulos, "Broadband dielectric characterization of high-permittivity rogers substrates via terahertz time-domain spectroscopy in reflection mode," *Appl. Sci.*, vol. 12, no. 16, p. 8259, Aug. 2022.
[35] M. D. Astorino, R. Fastampa, F. Frezza, L. Maiolo, M. Marrani, M. Missori, M. Muzi, N. Tedeschi, and A. Veroli, "Polarization-maintaining reflection-mode THz time-domain spectroscopy of a polyimide based ultra-thin narrow-band metamaterial absorber," *Sci. Rep.*, vol. 8, no. 1, p. 1985, Jan. 2018.
[36] Website Toptica, Oct. 2025. [Online]. Available: https://www.toptica.com/products/terahertz-systems

Edoardo Negri (Member, IEEE) was born in Orvieto, Italy, in 1997. He received the B.Sc. and M.Sc. degrees (cum laude) in electronic engineering, with honorable mention for the academic curriculum, from Sapienza University of Rome, Rome, Italy, in July 2019 and 2021, respectively. In the same institution he received, in January 2025, the Ph.D. degree (cum laude and the 'Doctor Europaeus' label) in Information and Communications Technologies (applied electromagnetics curriculum). From March to May 2023, he was a Visiting Ph.D. Student with the Institut d'Électronique et de Télécommunications de Rennes (IETR), Université de Rennes 1, Rennes, France. From September to November 2023, he was a visiting Ph.D. Student in Ferdinand-Braun-Institut, Leibniz-Institut fchstfrequenztechnik (FBH), Berlin, Germany. Since July 2024, Dr. Negri has been a Research Fellow at the Institute for Microelectronics and Microsystems (IMM) of the National Research Council (CNR), Rome, Italy. His main research interests include leaky waves, metasurfaces, focusing devices, wireless near-field links, and THz devices. Dr. Negri received the "Antonio Ventura" Award as one of the best engineering students at the Sapienza University of Rome in 2022, the IEEE Antennas and Propagation Society (APS) Fellowship Award in 2023 and 2025, the European Microwave Association (EuMA) Internship Award in 2023, an honorary mention in the "Barzilai Award" at the "Riunione Nazionale di Elettromagnetismo (RiNEm)" 2024, the second prize for the industrial call for ideas "Huawei TechArena", and the first prize at the "Best Student Paper Award" at the International Symposium on Antennas and Propagation (ISAP) in 2024.

Dimitrios C. Zografopoulos received the diploma in electrical engineering and the Doctorate degree from the School of Electrical and Computer Engineering, Aristotle University of Thessaloniki, Thessaloniki, Greece, in 2003 and 2009, respectively.

His doctoral thesis focused on the design and analysis of photonic crystal fibers with tunable polarization properties. In 2010, he was a Postdoctoral Fellow of the Research Committee of the AUTH and in 2011 a Postdoctoral Research Fellow of the Greek States Scholarship Foundation and a Visiting Research Fellow with the Department of Electronics Technology, Carlos III University of Madrid, Spain. The same year, he moved under an Intra-European Marie-Curie Fellowship to the Institute for Microelectronics and Microsystems (IMM) of the National Research Council of Italy (CNR). He was a Researcher with the Rome Unit of CNR-IMM till 2023, when he was promoted to a Senior Researcher. Since 2025, he has been an Associate Professor with the Department of Electrical and Computer Engineering, Aristotle University of Thessaloniki. He has authored or coauthored more than 120 scientific articles in international journals, 100 presentations in international conferences, and three book chapters. His current research interests include the investigation of strongly resonant metasurfaces, tunable metamaterials, components for THz wave manipulation, and the interaction between electromagnetic waves, and liquid crystals.

Francesco Maita received the M.Sc. (cum laude) degree in Electronics Engineering and the Ph.D. in "Engineering of Sensorial and Learning Systems" both from the "Università degli studi di Roma Tor Vergata", in 2008 and 2013, respectively. He worked as a post-doctoral researcher at the Institute for Microelectronics and Microsystems of the CNR of Rome from 2012 to 2016. Since 2017, he works as a researcher at the same institution. His research activity focuses on electronic design, fabrication and characterization of smart circuits for sensing, with a specific focus on flexible and biodegradable devices both from a material, device and system perspective. Since 2024 is a scientific panel expert for project evaluation of Polish National Science Centre.

Luca Maiolo received the Master degree in Physics in 2003 and the Ph.D. in 2008, both from "Università degli studi di RomaTre". In the 2004 he was a research assistant at Institute for Photonics and Nanotechnologies, working on fabrication and electrical characterization of polycrystalline thin film transistors for large area electronics applications. In 2009 he joined to Robotics, Brain and Cognitive Sciences Department of Italian Institute of Technology in Genova, as post-doctoral fellow, where he developed and tested tactile flexible sensors for humanoid robot. Currently, he works as senior researcher at the Institute for Microelectronics and Microsystems of the National Research Council (CNR-IMM). His activity is mainly focused on fabrication and characterization of smart systems integrated on ultrathin flexible substrates for biomedical, aerospace and industrial application with a special focus on sustainable process and biopolymers. He is co-founder of the interdisciplinary group TechforBio for the development of advanced devices and sensors in biomedical applications. Rapporteur for the Italian Ministries of Economic Development and Education University Research in the panel of Nanotechnologies. He is scientific expert for project evaluation in Polish National Science Centre, Dutch Research Council and for the European Commission. Currently, he is Associate Editor for Frontiers Bioengineering and Biotechnology, Review Editor for Frontiers in Electronics and Member of the editorial board for Biosensors.

Romeo Beccherelli (Member, IEEE) was born in Plovdiv, Bulgaria, in 1969. He received the Laurea (cum laude) and Ph.D. degrees in electronic engineering from the Sapienza University of Rome, Italy, in 1994 and 1998, respectively. In 1997, he joined as a Post-Doctoral Research Assistant with the Department of Engineering Science, University of Oxford, Oxford, U.K. In 2001, he was appointed as a Researcher, in 2006, a Senior Researcher, and the Director of Research in 2021 at the National Research Council of Italy, Institute for Microelectronics and Microsystems, Rome. He has invented two patents and authored of more than 100 scientific articles in international journals, more than 110 conference proceedings papers, and eight book chapters. He has been a Principal Investigator in research projects funded by European Community, European Space Agency, the Italian Government, and the industry, and the co-coordinator of four bilateral projects. His research interests include liquid crystal display technology have evolved into sensor arrays, photonics and plasmonics based on liquid crystals, and into metamaterial and metasurface devices, and systems for wireless communications in the microwaves and terahertz frequency ranges. His Ph.D. thesis was awarded the International Otto Lehman Prize 1999 in liquid crystal technology by the University of Karlsruhe, Germany, and the Otto Lehmann Foundation.

Walter Fuscaldo (Senior Member, IEEE) received the M.Sc. (cum laude) degree in Telecommunications Engineering from Sapienza University of Rome, Rome, in 2013. In 2017, he received the Ph.D. degree (cum laude and with the Doctor Europaeus label) in Information and Communication Technology (Applied Electromagnetics curriculum) from both the Department of Information Engineering, Electronics and Telecommunications (DIET), Sapienza University of Rome, and the Institut d'Électronique et de Télécommunications de Rennes (IETR), Université de Rennes 1, Rennes, France, under a cotutelle agreement between the institutions. In 2014, 2017, 2018, he was a Visiting Researcher and in 2023 a Visiting Scientist with the NATO-STO Center for Maritime Research and Experimentation (CMRE), La Spezia, Italy. In 2016, he was a Visiting PhD student with the University of Houston, Houston, TX, USA. From July 2017 to June 2020, he was a Research Fellow at Sapienza University of Rome, and in July 2020, he joined the Institute for Microelectronics and Microsystems (IMM), Rome of the National Research Council of Italy as a Researcher, where he is currently a Senior Researcher since 2023. His current research interests include propagation of leaky, surface, and plasmonic waves, analysis and design of leaky-wave antennas, generation of electromagnetic localized waves, THz technology and spectroscopy, graphene electromagnetics, and metasurfaces. Dr. Fuscaldo was awarded several prizes, among which is the prestigious EuRAAP Leopold B. Felsen Award for Excellence in Electrodynamics in 2025. Since 2021 he has been included in the World's Top 2% Scientists' list by Stanford University. He is currently an Associate Editor of the journals Nature - Scientific Reports, IET - Microwaves, Antennas and Propagation, and IET - Electronics Letters.